

Spin dynamics in HTSC cuprates: The singlet–correlated band (or t-J-V) model and its applications

T. Mayer,¹ M. Eremin,² I. Eremin,^{3,4} and P. F. Meier¹

¹*Physics Institute, University of Zurich, CH-8055 Zurich, Switzerland*

²*Kazan State University, Kazan 420008, Russia*

³*Max-Planck Institut für Physik komplexer Systeme, D-01187 Dresden, Germany*

⁴*Technische Universität Braunschweig, D-38106 Braunschweig, Germany*

So far calculations of the spin susceptibility in the superconducting state of cuprates have been performed in the framework of weak–coupling approximations. However, it is known that cuprates belong to Mott–Hubbard doped materials where electron correlations are important. In this paper an analytical expression for the spin susceptibility in the superconducting state of cuprates is derived within the singlet–correlated band model, which takes into account strong correlations. The expression of the spin susceptibility is evaluated using values for the hopping parameters adapted to measurements of the Fermi surface of the materials $\text{YBa}_2\text{Cu}_3\text{O}_7$ and $\text{Bi}_2\text{Sr}_2\text{CaCu}_2\text{O}_8$. We show that the available experimental data which are directly related to the spin susceptibility can be explained consistently within one set of model parameters for each material. These experiments include the magnetic resonance peak observed by inelastic neutron scattering and the temperature dependence of the NMR spin shift, spin–spin and spin–lattice relaxation rates in the superconducting state.

PACS numbers: 74.25.Ha, 74.72.-h, 74.20.Mn, 74.25.Nf

I. INTRODUCTION

Derivations of theoretical expressions for the dynamical spin susceptibility of layered cuprates have been the focus of many ongoing investigations, since various experimental quantities are directly related to the spin susceptibility. Large amount of data sets exist on the temperature dependence of the Knight shift, spin–spin and spin–lattice relaxation rates as well as inelastic neutron scattering (INS) measurements. The most complete set of experimental data has been obtained for the YBaCuO compounds.

The theoretical approaches to the spin susceptibility can be divided into two categories, the weak– and strong–coupling models. The former deals with a single–band Hubbard model with the effective Coulomb interaction U_e taken to be of the order of the bandwidth in cuprates. Based on this assumption, the dynamical spin susceptibility can be calculated within a standard random phase approximation (RPA) approach. Extensive studies of NMR data were carried out within the framework of this model by Bulut and Scalapino et al.^{1,2,3,4,5} and Mack et al.⁶. In the meantime, the features observed by inelastic neutron scattering were studied theoretically by several groups^{7,8}. However, in all of these calculations the effect of strong electronic correlations were not taken into account properly.

At the same time, there were a number of studies devoted to analyzing the spin susceptibility within the strong–coupling t–J model, for which standard many–body perturbative methods do not work. For example the dynamical spin susceptibility was analyzed within the slave–boson approximation⁹, Mori–Zwanzig memory function formalism¹⁰ and with the Hubbard X–operators

technique^{11,12}. It has been found that to a large extent, both weak and strong–coupling calculations give very similar results for the spin susceptibility. The respective parameter values, however, differ drastically. Until now, there is no complete understanding whether both INS and NMR data can be explained consistently within one model and using the same parameter values of the given theory.

In the present work we analyze this question in detail. Starting from the singlet–correlated band model, we use a well established decoupling procedure of the equations of motion and approximate higher order correlation functions so as to obtain an analytical expression for the dynamical spin susceptibility which takes into account strong correlations. It has been found by Hubbard and Jain¹³ that the expression for the dynamical susceptibility has a non–trivial correction due to strong correlation effects. Later Zavidonov and Brinkmann¹¹ have incorporated an additional functional correction for the lower Hubbard sub–band (LHB) model, which accounts for local spin fluctuation effects. Both of these corrections are different from the conventional Pauli–Lindhard form and therefore they cannot be exactly included in the RPA approach.

In the present paper we extend the previous analysis and present an analytical expression for the dynamical spin susceptibility in the upper Hubbard sub–band (UHB) in the superconducting state. We perform an extended numerical evaluation of this analytical expression and find that most of the available experimental data which are directly related to the spin susceptibility can be explained consistently within one set of model parameters. These experiments include the magnetic resonance peak observed by INS and the temperature dependence

of the NMR spin shift, spin–spin and the spin–lattice relaxation rates, measured in the superconducting state. Note that in our analysis we restrict ourselves to optimally doped high–temperature superconductors, since the pseudogap phenomenon cannot be explained within our model. Furthermore, in our analysis we take advantage of other available experiments, like the Fermi surface topology in various cuprate superconductors that is determined by high–resolution angle–resolved photoemission. Assuming a $d_{x^2-y^2}$ –wave pairing symmetry, we propose an optimal set of parameters for the $\text{YBa}_2\text{Cu}_3\text{O}_7$ and $\text{Bi}_2\text{Sr}_2\text{CaCu}_2\text{O}_8$ compounds.

This paper is organized as follows. In Sec. II we introduce the model system and present the analytical expression for the spin susceptibility in the superconducting state of cuprates. In Sec. III and Sec. IV we study the spin susceptibility in the singlet–correlated band model by analyzing experiments in the superconducting state of the materials $\text{YBa}_2\text{Cu}_3\text{O}_7$ and $\text{Bi}_2\text{Sr}_2\text{CaCu}_2\text{O}_8$. Summary and conclusions are given in Sec. V.

II. DYNAMICAL SPIN SUSCEPTIBILITY IN THE SINGLET–CORRELATED BAND MODEL

The starting point for our calculation is the model Hamiltonian^{12,14}

$$H = \sum_{i,j,\sigma} t_{ij} \psi_i^{pd,\sigma} \psi_j^{\sigma,pd} + \sum_{i>j} J_{ij} \left[(\mathbf{S}_i \mathbf{S}_j) - \frac{n_i n_j}{4} \right] \quad (1)$$

$$+ \sum_{i>j} V_{ij} \delta_i \delta_j,$$

where $\psi_i^{pd,\sigma}$ ($\psi_i^{\sigma,pd}$) are composite copper–oxygen creation (annihilation) operators of the copper–oxygen singlet¹⁵ states in the CuO_2 –plane. Furthermore J_{ij} is the superexchange parameter of the copper spins (this coupling originates from the virtual hopping from LHB to UHB via the oxygen state). The number of doped holes is described by $\delta_i = \psi_i^{pd,pd}$ and V_{ij} is an effective density–density interaction parameter. This parameter allows to account for the screened Coulomb repulsion and phonon (or plasmon) mediated interactions as well. Consequently, the last term is a Coulomb–like interaction between doped holes, which can be neglected, because it does not contribute to the spin susceptibility.

The susceptibility is calculated from the general expression

$$\chi^{+-}(\mathbf{q}, \omega) = -2\pi i \langle \langle S_{\mathbf{q}}^+ | S_{-\mathbf{q}}^- \rangle \rangle, \quad (2)$$

where the spin density operator $S_{\mathbf{q}}^+$ for the singlet–correlated band is written as

$$S_{\mathbf{q}}^+ = \sum_{\mathbf{k}} \left(\psi_{\mathbf{k}}^{\uparrow,0} + \psi_{\mathbf{k}}^{pd,\downarrow} \right) \left(\psi_{\mathbf{k}+\mathbf{q}}^{0,\downarrow} - \psi_{\mathbf{k}+\mathbf{q}}^{\uparrow,pd} \right) \quad (3)$$

$$\simeq - \sum_{\mathbf{k}} \psi_{\mathbf{k}}^{pd,\downarrow} \psi_{\mathbf{k}+\mathbf{q}}^{\uparrow,pd}.$$

Here we neglected all the quasiparticle creation (annihilation) operators $\psi_i^{0,\sigma}$ ($\psi_i^{\sigma,0}$) corresponding to the LHB, because this band is assumed to be completely filled.

The expression for the susceptibility is derived by the following procedure. First, we write down a complete set of equations of motion using the composite copper–oxygen creation (annihilation) operators $\psi_i^{pd,\sigma}$ ($\psi_i^{\sigma,pd}$) of the copper–oxygen singlet states in the plane. Then, by means of a linear transformation we rearrange these equations via Bogoliubov’s quasiparticle operators into new sets of equations, which finally will be solved. An expression for the susceptibility was previously derived¹⁴ by utilizing the method of Heisenberg equations of motion in a small magnetic field. The advantage of the Green’s function method is that it allows to obtain a formula for the susceptibility which contains both the itinerant (or quasi Fermi–liquid) part and the local spin fluctuation part in one general expression.

The equation of motion for the relevant Green’s function in the normal state ($T > T_c$) has been derived before by some of us¹². It is given by

$$\omega \langle \langle -\psi_{\mathbf{k}}^{pd,\downarrow} \psi_{\mathbf{k}+\mathbf{q}}^{\uparrow,pd} | S_{-\mathbf{q}}^- \rangle \rangle = \quad (4)$$

$$\frac{i}{2\pi} \left(\langle \psi_{\mathbf{k}}^{pd,\downarrow} \psi_{\mathbf{k}}^{\downarrow,pd} \rangle - \langle \psi_{\mathbf{k}+\mathbf{q}}^{pd,\uparrow} \psi_{\mathbf{k}+\mathbf{q}}^{\uparrow,pd} \rangle \right)$$

$$- (\varepsilon_{\mathbf{k}} - \varepsilon_{\mathbf{k}+\mathbf{q}}) \langle \langle -\psi_{\mathbf{k}}^{pd,\downarrow} \psi_{\mathbf{k}+\mathbf{q}}^{\uparrow,pd} | S_{-\mathbf{q}}^- \rangle \rangle$$

$$+ \frac{1}{N} \left\{ (J_{\mathbf{q}} - t_{\mathbf{k}}) \langle \psi_{\mathbf{k}}^{\downarrow,pd} \psi_{\mathbf{k}}^{pd,\downarrow} \rangle \right.$$

$$\left. - (J_{\mathbf{q}} - t_{\mathbf{k}+\mathbf{q}}) \langle \psi_{\mathbf{k}+\mathbf{q}}^{pd,\uparrow} \psi_{\mathbf{k}+\mathbf{q}}^{\uparrow,pd} \rangle \right\} \langle \langle S_{\mathbf{q}}^+ | S_{-\mathbf{q}}^- \rangle \rangle$$

$$+ \frac{P}{N} \sum_{\mathbf{k}'} (t_{\mathbf{k}'+\mathbf{q}} - t_{\mathbf{k}'}) \langle \langle \psi_{\mathbf{k}'}^{pd,\downarrow} \psi_{\mathbf{k}'+\mathbf{q}}^{\uparrow,pd} | S_{-\mathbf{q}}^- \rangle \rangle,$$

where the factor $P = (1 + \delta)/2$ is a doping dependent constant which arises due to the narrowing of the band in the so–called Hubbard–I approximation.

In addition to Eq. (4) it has been shown¹² that

$$\omega \langle \langle S_{\mathbf{q}}^+ | S_{-\mathbf{q}}^- \rangle \rangle = \quad (5)$$

$$\sum_{\mathbf{k}'} (t_{\mathbf{k}'} - t_{\mathbf{k}'+\mathbf{q}}) \langle \langle \psi_{\mathbf{k}'}^{pd,\downarrow} \psi_{\mathbf{k}'+\mathbf{q}}^{\uparrow,pd} | S_{-\mathbf{q}}^- \rangle \rangle.$$

Therefore, if we combine Eq. (4) and Eq. (5) we get

$$\omega \langle \langle -\psi_{\mathbf{k}}^{pd,\downarrow} \psi_{\mathbf{k}+\mathbf{q}}^{\uparrow,pd} | S_{-\mathbf{q}}^- \rangle \rangle = \quad (6)$$

$$\frac{i}{2\pi} \left(\langle \psi_{\mathbf{k}}^{pd,\downarrow} \psi_{\mathbf{k}}^{\downarrow,pd} \rangle - \langle \psi_{\mathbf{k}+\mathbf{q}}^{pd,\uparrow} \psi_{\mathbf{k}+\mathbf{q}}^{\uparrow,pd} \rangle \right)$$

$$- (\varepsilon_{\mathbf{k}} - \varepsilon_{\mathbf{k}+\mathbf{q}}) \langle \langle -\psi_{\mathbf{k}}^{pd,\downarrow} \psi_{\mathbf{k}+\mathbf{q}}^{\uparrow,pd} | S_{-\mathbf{q}}^- \rangle \rangle$$

$$\begin{aligned}
& + \frac{1}{N} \left\{ (J_{\mathbf{q}} - t_{\mathbf{k}}) \left\langle \psi_{\mathbf{k}}^{\downarrow, pd} \psi_{\mathbf{k}}^{pd, \downarrow} \right\rangle \right. \\
& - (J_{\mathbf{q}} - t_{\mathbf{k}+\mathbf{q}}) \left\langle \psi_{\mathbf{k}+\mathbf{q}}^{pd, \uparrow} \psi_{\mathbf{k}+\mathbf{q}}^{\uparrow, pd} \right\rangle \left. \right\} \langle \langle S_{\mathbf{q}}^+ | S_{-\mathbf{q}}^- \rangle \rangle \\
& - \frac{P}{N} \omega \langle \langle S_{\mathbf{q}}^+ | S_{-\mathbf{q}}^- \rangle \rangle.
\end{aligned}$$

The equation of motion (6) allows to derive the expression of the dynamical spin susceptibility in the normal state¹².

For the superconducting state we need to perform Bogoliubov's transformation

$$\begin{aligned}
\alpha_{\mathbf{k}}^{pd, \downarrow} &= u_{\mathbf{k}} \psi_{\mathbf{k}}^{pd, \downarrow} - v_{\mathbf{k}} \psi_{-\mathbf{k}}^{\uparrow, pd} \\
\alpha_{\mathbf{k}}^{pd, \uparrow} &= u_{\mathbf{k}} \psi_{\mathbf{k}}^{pd, \uparrow} + v_{\mathbf{k}} \psi_{-\mathbf{k}}^{\downarrow, pd}.
\end{aligned} \quad (7)$$

Consequently, the spin operator for the superconducting state will be written as

$$\begin{aligned}
S_{\mathbf{q}}^+ &= \\
& - \sum_{\mathbf{k}} \left(u_{\mathbf{k}+\mathbf{q}} u_{\mathbf{k}} \alpha_{\mathbf{k}}^{pd, \downarrow} \alpha_{\mathbf{k}+\mathbf{q}}^{\uparrow, pd} + v_{\mathbf{k}} u_{\mathbf{k}+\mathbf{q}} \alpha_{-\mathbf{k}}^{\uparrow, pd} \alpha_{\mathbf{k}+\mathbf{q}}^{\uparrow, pd} \right) \\
& + \sum_{\mathbf{k}} \left(u_{\mathbf{k}} v_{\mathbf{k}+\mathbf{q}} \alpha_{\mathbf{k}}^{pd, \downarrow} \alpha_{-\mathbf{k}-\mathbf{q}}^{pd, \downarrow} + v_{\mathbf{k}} v_{\mathbf{k}+\mathbf{q}} \alpha_{-\mathbf{k}}^{\uparrow, pd} \alpha_{-\mathbf{k}-\mathbf{q}}^{pd, \downarrow} \right).
\end{aligned} \quad (8)$$

Therefore in the superconducting state we need to construct additional equations for the Green's functions $\langle \langle -\alpha_{\mathbf{k}}^{pd, \downarrow} \alpha_{\mathbf{k}+\mathbf{q}}^{\uparrow, pd} | S_{-\mathbf{q}}^- \rangle \rangle$, $\langle \langle -\alpha_{-\mathbf{k}}^{\uparrow, pd} \alpha_{\mathbf{k}+\mathbf{q}}^{\uparrow, pd} | S_{-\mathbf{q}}^- \rangle \rangle$, $\langle \langle \alpha_{\mathbf{k}}^{pd, \downarrow} \alpha_{-\mathbf{k}-\mathbf{q}}^{pd, \downarrow} | S_{-\mathbf{q}}^- \rangle \rangle$ and $\langle \langle \alpha_{-\mathbf{k}}^{\uparrow, pd} \alpha_{-\mathbf{k}-\mathbf{q}}^{pd, \downarrow} | S_{-\mathbf{q}}^- \rangle \rangle$.

Each of them has to be expressed via the $\psi_{\mathbf{k}}^{pd, \sigma}$ operators, for example

$$\begin{aligned}
\langle \langle -\alpha_{\mathbf{k}}^{pd, \downarrow} \alpha_{\mathbf{k}+\mathbf{q}}^{\uparrow, pd} | S_{-\mathbf{q}}^- \rangle \rangle &= \\
& - u_{\mathbf{k}} u_{\mathbf{k}+\mathbf{q}} \langle \langle \psi_{\mathbf{k}}^{pd, \downarrow} \psi_{\mathbf{k}+\mathbf{q}}^{\uparrow, pd} | S_{-\mathbf{q}}^- \rangle \rangle \\
& + v_{\mathbf{k}} u_{\mathbf{k}+\mathbf{q}} \langle \langle \psi_{-\mathbf{k}}^{\uparrow, pd} \psi_{\mathbf{k}+\mathbf{q}}^{\uparrow, pd} | S_{-\mathbf{q}}^- \rangle \rangle \\
& - u_{\mathbf{k}} v_{\mathbf{k}+\mathbf{q}} \langle \langle \psi_{\mathbf{k}}^{pd, \downarrow} \psi_{-\mathbf{k}-\mathbf{q}}^{pd, \downarrow} | S_{-\mathbf{q}}^- \rangle \rangle \\
& + v_{\mathbf{k}} v_{\mathbf{k}+\mathbf{q}} \langle \langle \psi_{-\mathbf{k}}^{\uparrow, pd} \psi_{-\mathbf{k}-\mathbf{q}}^{pd, \downarrow} | S_{-\mathbf{q}}^- \rangle \rangle.
\end{aligned} \quad (9)$$

Doing so we get

$$\begin{aligned}
\omega \langle \langle -\psi_{\mathbf{k}}^{pd, \downarrow} \psi_{\mathbf{k}+\mathbf{q}}^{\uparrow, pd} | S_{-\mathbf{q}}^- \rangle \rangle &= \\
& \frac{i}{2\pi} \left(\langle \langle \psi_{\mathbf{k}}^{pd, \downarrow} \psi_{\mathbf{k}}^{\downarrow, pd} \rangle \rangle - \langle \langle \psi_{\mathbf{k}+\mathbf{q}}^{pd, \uparrow} \psi_{\mathbf{k}+\mathbf{q}}^{\uparrow, pd} \rangle \rangle \right) \\
& + \langle \langle [-\psi_{\mathbf{k}}^{pd, \downarrow} \psi_{\mathbf{k}+\mathbf{q}}^{\uparrow, pd}, H] | S_{-\mathbf{q}}^- \rangle \rangle_{tr} \\
& + \frac{1}{N} \left\{ (J_{\mathbf{q}} - t_{\mathbf{k}}) \left\langle \psi_{\mathbf{k}}^{\downarrow, pd} \psi_{\mathbf{k}}^{pd, \downarrow} \right\rangle \right.
\end{aligned} \quad (10)$$

$$\begin{aligned}
& - (J_{\mathbf{q}} - t_{\mathbf{k}+\mathbf{q}}) \left\langle \psi_{\mathbf{k}+\mathbf{q}}^{pd, \uparrow} \psi_{\mathbf{k}+\mathbf{q}}^{\uparrow, pd} \right\rangle \left. \right\} \langle \langle S_{\mathbf{q}}^+ | S_{-\mathbf{q}}^- \rangle \rangle \\
& - \frac{P}{N} \omega \langle \langle S_{\mathbf{q}}^+ | S_{-\mathbf{q}}^- \rangle \rangle,
\end{aligned}$$

and similar expressions can be obtained for $\langle \langle \psi_{-\mathbf{k}}^{\uparrow, pd} \psi_{\mathbf{k}+\mathbf{q}}^{\uparrow, pd} | S_{-\mathbf{q}}^- \rangle \rangle$, $\langle \langle \psi_{\mathbf{k}}^{pd, \downarrow} \psi_{-\mathbf{k}-\mathbf{q}}^{pd, \downarrow} | S_{-\mathbf{q}}^- \rangle \rangle$ and $\langle \langle \psi_{-\mathbf{k}}^{\uparrow, pd} \psi_{-\mathbf{k}-\mathbf{q}}^{pd, \downarrow} | S_{-\mathbf{q}}^- \rangle \rangle$. Equation (10) has the same form as in the normal state (Eq. (6)), except that it is now adapted to be applied for the superconducting state. We note that in the conventional Fermi-liquid theory the anticommutator rule is given as $c_{\mathbf{k}\sigma} c_{\mathbf{k}\sigma}^{\dagger} + c_{\mathbf{k}\sigma}^{\dagger} c_{\mathbf{k}\sigma} = 1$. In the strong-coupling limit, however, this rule is modified¹⁶ due to the Coulomb repulsion. For this reason we have abbreviated the terms which are present in the conventional weak-coupling Fermi-liquid approach in the superconducting state by the truncated Green's function $\langle \langle [-\psi_{\mathbf{k}}^{pd, \downarrow} \psi_{\mathbf{k}+\mathbf{q}}^{\uparrow, pd}, H] | S_{-\mathbf{q}}^- \rangle \rangle_{tr}$. The other terms on the right hand side of Eq. (10) are due to the spin modulation $S_{\mathbf{q}}^+$.

With the help of these equations we are able to construct the equations of motion which are needed to calculate the spin susceptibility in the superconducting state. The first one is given as

$$\begin{aligned}
(\omega - E_{\mathbf{p}} + E_{\mathbf{k}}) \langle \langle \alpha_{\mathbf{k}}^{pd, \downarrow} \alpha_{\mathbf{p}}^{\uparrow, pd} | S_{-\mathbf{q}}^- \rangle \rangle &= \\
& \frac{i}{2\pi} (u_{\mathbf{k}} u_{\mathbf{p}} + v_{\mathbf{k}} v_{\mathbf{p}}) (n_{\mathbf{p}} - n_{\mathbf{k}}) \\
& + \frac{1}{N} (u_{\mathbf{k}} u_{\mathbf{p}} + v_{\mathbf{k}} v_{\mathbf{p}}) \{ (J_{\mathbf{q}} - t_{\mathbf{p}}) n_{\mathbf{p}} \\
& - (J_{\mathbf{q}} - t_{\mathbf{k}}) n_{\mathbf{k}} \} \langle \langle S_{\mathbf{q}}^+ | S_{-\mathbf{q}}^- \rangle \rangle \\
& + (P u_{\mathbf{k}} u_{\mathbf{p}} + (P - 1) v_{\mathbf{k}} v_{\mathbf{p}}) \frac{\omega}{N} \langle \langle S_{\mathbf{q}}^+ | S_{-\mathbf{q}}^- \rangle \rangle,
\end{aligned} \quad (11)$$

and similar expressions occur for $\langle \langle \alpha_{-\mathbf{k}}^{\uparrow, pd} \alpha_{-\mathbf{p}}^{pd, \downarrow} | S_{-\mathbf{q}}^- \rangle \rangle$, $\langle \langle \alpha_{-\mathbf{k}}^{\uparrow, pd} \alpha_{\mathbf{p}}^{\uparrow, pd} | S_{-\mathbf{q}}^- \rangle \rangle$ and $\langle \langle \alpha_{\mathbf{k}}^{pd, \downarrow} \alpha_{-\mathbf{p}}^{pd, \downarrow} | S_{-\mathbf{q}}^- \rangle \rangle$. Furthermore, $n_{\mathbf{k}} = \langle \alpha_{\mathbf{k}}^{pd, \uparrow} \alpha_{\mathbf{k}}^{\uparrow, pd} \rangle = \langle \alpha_{\mathbf{k}}^{pd, \downarrow} \alpha_{\mathbf{k}}^{\downarrow, pd} \rangle$ are the occupation numbers in the superconducting state. We further make use of the identity

$$\begin{aligned}
\langle \langle S_{\mathbf{q}}^+ | S_{-\mathbf{q}}^- \rangle \rangle &= \\
& - \sum_{\mathbf{k}} u_{\mathbf{k}+\mathbf{q}} u_{\mathbf{k}} \langle \langle \alpha_{\mathbf{k}}^{pd, \downarrow} \alpha_{\mathbf{k}+\mathbf{q}}^{\uparrow, pd} | S_{-\mathbf{q}}^- \rangle \rangle \\
& + \sum_{\mathbf{k}} v_{\mathbf{k}+\mathbf{q}} u_{\mathbf{k}} \langle \langle \alpha_{\mathbf{k}}^{pd, \downarrow} \alpha_{-\mathbf{k}-\mathbf{q}}^{pd, \downarrow} | S_{-\mathbf{q}}^- \rangle \rangle \\
& - \sum_{\mathbf{k}} u_{\mathbf{k}+\mathbf{q}} v_{\mathbf{k}} \langle \langle \alpha_{-\mathbf{k}}^{\uparrow, pd} \alpha_{\mathbf{k}+\mathbf{q}}^{\uparrow, pd} | S_{-\mathbf{q}}^- \rangle \rangle \\
& + \sum_{\mathbf{k}} v_{\mathbf{k}+\mathbf{q}} v_{\mathbf{k}} \langle \langle \alpha_{-\mathbf{k}}^{\uparrow, pd} \alpha_{-\mathbf{k}-\mathbf{q}}^{pd, \downarrow} | S_{-\mathbf{q}}^- \rangle \rangle.
\end{aligned} \quad (12)$$

With help of this relation the susceptibility is calculated as

$$\chi^{+,-}(\mathbf{q}, \omega) = \frac{\chi_0^{+,-}(\mathbf{q}, \omega)}{1 + J_{\mathbf{q}}\chi_0^{+,-}(\mathbf{q}, \omega) + \Pi(\mathbf{q}, \omega) + Z(\mathbf{q}, \omega)}, \quad (13)$$

where the superexchange interaction between the copper spins is $J_{\mathbf{q}} = J_1(\cos q_x + \cos q_y)$, with J_1 being the superexchange interaction parameter between the nearest neighbour copper spins. The function $\chi_0^{+,-}(\mathbf{q}, \omega)$ is a BCS-like susceptibility and $\Pi(\mathbf{q}, \omega)$ is a function which results from strong correlation effects and has been determined¹⁴ before. It is given by

$$\begin{aligned} \Pi(\mathbf{q}, \omega) = & \frac{P}{N} \sum_{\mathbf{k}} (x_{\mathbf{k}}x_{\mathbf{k}+\mathbf{q}} \\ & + z_{\mathbf{k}}z_{\mathbf{k}+\mathbf{q}}) \frac{t_{\mathbf{k}}f_{\mathbf{k}} - t_{\mathbf{k}+\mathbf{q}}f_{\mathbf{k}+\mathbf{q}}}{\omega + i\Gamma + E_{\mathbf{k}} - E_{\mathbf{k}+\mathbf{q}}} \\ & + \frac{P}{N} \sum_{\mathbf{k}} (y_{\mathbf{k}}y_{\mathbf{k}+\mathbf{q}} \\ & + z_{\mathbf{k}}z_{\mathbf{k}+\mathbf{q}}) \frac{t_{\mathbf{k}}(1 - f_{\mathbf{k}}) - t_{\mathbf{k}+\mathbf{q}}(1 - f_{\mathbf{k}+\mathbf{q}})}{\omega + i\Gamma - E_{\mathbf{k}} + E_{\mathbf{k}+\mathbf{q}}} \\ & + \frac{P}{N} \sum_{\mathbf{k}} (x_{\mathbf{k}}y_{\mathbf{k}+\mathbf{q}} \\ & - z_{\mathbf{k}}z_{\mathbf{k}+\mathbf{q}}) \frac{t_{\mathbf{k}}f_{\mathbf{k}} - t_{\mathbf{k}+\mathbf{q}}(1 - f_{\mathbf{k}+\mathbf{q}})}{\omega + i\Gamma + E_{\mathbf{k}} + E_{\mathbf{k}+\mathbf{q}}} \\ & + \frac{P}{N} \sum_{\mathbf{k}} (y_{\mathbf{k}}x_{\mathbf{k}+\mathbf{q}} \\ & - z_{\mathbf{k}}z_{\mathbf{k}+\mathbf{q}}) \frac{t_{\mathbf{k}}(1 - f_{\mathbf{k}}) - t_{\mathbf{k}+\mathbf{q}}f_{\mathbf{k}+\mathbf{q}}}{\omega + i\Gamma - E_{\mathbf{k}} - E_{\mathbf{k}+\mathbf{q}}}. \end{aligned} \quad (14)$$

The function $Z(\mathbf{q}, \omega)$ has its origin in the fast fluctuation of the localized spins and it is calculated as

$$\begin{aligned} Z(\mathbf{q}, \omega) = & \frac{1}{N} \sum_{\mathbf{k}} (Px_{\mathbf{k}}x_{\mathbf{k}+\mathbf{q}} \\ & + (P-1)z_{\mathbf{k}}z_{\mathbf{k}+\mathbf{q}}) \frac{\omega + i\Gamma}{\omega + i\Gamma + E_{\mathbf{k}} - E_{\mathbf{k}+\mathbf{q}}} \\ & + \frac{1}{N} \sum_{\mathbf{k}} (Py_{\mathbf{k}}y_{\mathbf{k}+\mathbf{q}} \\ & + (P-1)z_{\mathbf{k}}z_{\mathbf{k}+\mathbf{q}}) \frac{\omega + i\Gamma}{\omega + i\Gamma - E_{\mathbf{k}} + E_{\mathbf{k}+\mathbf{q}}} \\ & + \frac{1}{N} \sum_{\mathbf{k}} (Px_{\mathbf{k}}y_{\mathbf{k}+\mathbf{q}} \\ & - (P-1)z_{\mathbf{k}}z_{\mathbf{k}+\mathbf{q}}) \frac{\omega + i\Gamma}{\omega + i\Gamma + E_{\mathbf{k}} + E_{\mathbf{k}+\mathbf{q}}} \\ & + \frac{1}{N} \sum_{\mathbf{k}} (Py_{\mathbf{k}}x_{\mathbf{k}+\mathbf{q}} \\ & - (P-1)z_{\mathbf{k}}z_{\mathbf{k}+\mathbf{q}}) \frac{\omega + i\Gamma}{\omega + i\Gamma - E_{\mathbf{k}} - E_{\mathbf{k}+\mathbf{q}}}, \end{aligned} \quad (15)$$

where the functions $x_{\mathbf{k}} = u_{\mathbf{k}}^2 = \frac{1}{2}(1 + \varepsilon_{\mathbf{k}}/E_{\mathbf{k}})$, $y_{\mathbf{k}} = v_{\mathbf{k}}^2 = \frac{1}{2}(1 - \varepsilon_{\mathbf{k}}/E_{\mathbf{k}})$ and $z_{\mathbf{k}} = u_{\mathbf{k}}v_{\mathbf{k}} = \Delta_{\mathbf{k}}/(2E_{\mathbf{k}})$ are the conventional coherence factors. Furthermore Γ is an artificially introduced damping constant and $E_{\mathbf{k}} = \sqrt{(\varepsilon_{\mathbf{k}} - \mu)^2 + \Delta_{\mathbf{k}}^2}$ is the energy of Bogoliubov's quasiparticles in the superconducting state. The energy dispersion in tight-binding approximation for a quadratic two-dimensional lattice is given as

$$\begin{aligned} \varepsilon_{\mathbf{k}} = & P[2t_1(\cos k_x + \cos k_y) \\ & + 4t_2(\cos k_x \cos k_y) \\ & + 2t_3(\cos 2k_x + \cos 2k_y) \\ & + 2t_4(\cos 2k_x \cos k_y + \cos 2k_y \cos k_x) \\ & + 4t_5(\cos 2k_x \cos 2k_y)], \end{aligned} \quad (16)$$

where the model parameters t_1, t_2, \dots correspond to nearest-neighbour (NN), next-nearest-neighbour (NNN), and further distant hopping, respectively. For simplicity we do not consider hopping between layers. Further we note that at optimal doping the number of doped holes per unit cell in one CuO_2 -layer is 0.165. In bilayer compounds therefore we have $\delta = 0.33$ with a corresponding factor $P = (1 + \delta)/2 \simeq 0.7$ near optimal doping.

The mechanism that causes the pairing in cuprates is still being debated and the origin of the interactions described by V_{ij} in Eq. (1) are unknown. Therefore we have introduced the superconducting gap function $\Delta_{\mathbf{k}}$ phenomenologically into our model. Assuming a $d_{x^2-y^2}$ pairing symmetry it is given by

$$\Delta_{\mathbf{k}}(T) = \frac{\Delta_0}{2} (\cos k_x - \cos k_y) \tanh\left(1.76\sqrt{T_c/T - 1}\right), \quad (17)$$

where Δ_0 is considered to be a model parameter. We would like to point out that this formula is a fit to the solution of the Eliashberg strong-coupling gap equation.

In the forthcoming sections we will analyze several experiments in the superconducting state of the materials $\text{YBa}_2\text{Cu}_3\text{O}_7$ and $\text{Bi}_2\text{Sr}_2\text{CaCu}_2\text{O}_8$. We would like to summarize at this point the parameters which we used to perform our analysis. The tight-binding hopping parameters ($Pt_1 \dots Pt_5$) are adopted from fits to the measured Fermi surfaces of these two materials. For $\text{YBa}_2\text{Cu}_3\text{O}_7$ we have¹⁷ $(\mu, Pt_1 \dots Pt_5) = (119, 147, -36.5, -2.4, 32.4, -1.8)$ meV, while for $\text{Bi}_2\text{Sr}_2\text{CaCu}_2\text{O}_8$ we take¹⁸ $(\mu, Pt_1 \dots Pt_5) = (49.4, 73.9, -12.0, 16.3, 6.3, -11.7)$ meV. The corresponding Fermi surfaces are shown in Fig. 1. Note that they are quite different for these two materials.

Other model parameters include the gap parameter which is assumed to be in the order of $\Delta_0 \simeq 10 - 30$ meV and the superexchange interaction parameter of the copper spins which is $J_1 \simeq 100 - 140$ meV. In our analysis

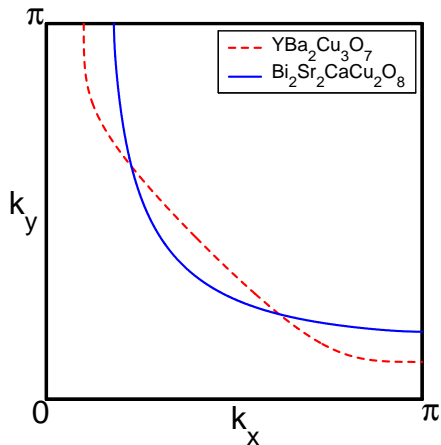


Figure 1: Fermi surfaces of $\text{YBa}_2\text{Cu}_3\text{O}_7$ (dashed) and $\text{Bi}_2\text{Sr}_2\text{CaCu}_2\text{O}_8$ (solid) according to photoemission experiments.

we proceed as follows. We assume the Fermi surface as given from fits to photoemission data and thus fix the values of the hopping parameters for both materials. Based on this assumption we analyze neutron scattering experiments which allows us to determine the values of the model parameters Δ_0 and J_1 . Then we move to NMR experiments and calculate the temperature dependences of spin shift, spin-spin relaxation and spin-lattice relaxation rates, utilizing the parameter values obtained before. Thus in our analysis we try to establish a connection between the different experiments.

III. NEUTRON SCATTERING ANALYSIS

Magnetic inelastic neutron scattering experiments probe directly the imaginary part of the dynamical spin susceptibility $\text{Im}\chi^{+,-}(\mathbf{q}, \omega)$. The experiments indicate a sharp resonance in the magnetic excitation spectrum of optimally doped $\text{YBa}_2\text{Cu}_3\text{O}_7$ ^{19,20} and $\text{Bi}_2\text{Sr}_2\text{CaCu}_2\text{O}_8$ ^{21,22} compounds at a frequency $\omega \simeq 41$ meV, near the antiferromagnetic wave vector $\mathbf{Q} = (\pi, \pi)$. Consequently, there should be a large peak in the imaginary part of the spin susceptibility $\text{Im}\chi^{+,-}(\mathbf{Q}, \omega)$ at the same frequency. In the conventional weak-coupling scenario this feature was studied extensively by various authors^{7,8}, who connected the appearance of the resonance peak to a collective spin-density wave mode formation. Special experimental features like the effect of orthorhombic distortions²³ and bilayer splitting²⁴ on the magnetic excitations were also studied theoretically^{25,26} within the weak-coupling model. In the strong-coupling limit previous calculations were carried out by some of us¹⁴ and the dependence of the position of the resonance peak on the model parameters was studied extensively. We will not repeat these considerations here. Note only that within our

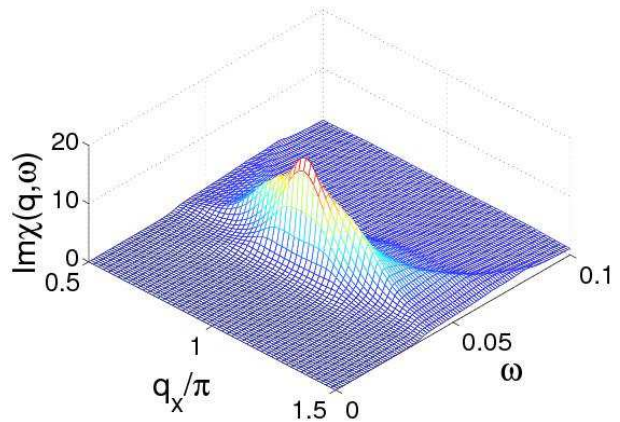
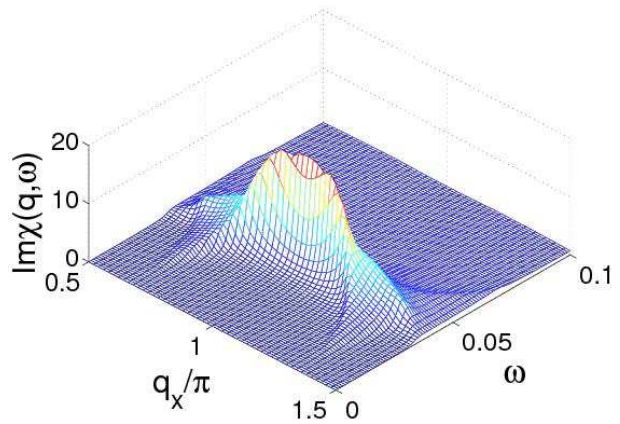


Figure 2: Calculated frequency and momentum dependence of $\text{Im}\chi^{+,-}(\mathbf{q}, \omega)$ for $\text{YBa}_2\text{Cu}_3\text{O}_7$ (top) and $\text{Bi}_2\text{Sr}_2\text{CaCu}_2\text{O}_8$ (bottom).

model the position of the neutron scattering resonance peak is determined mainly by the magnitude of the superconducting gap Δ_0 and the superexchange parameter J_1 . In particular, the superconducting gap parameter Δ_0 determines the size of the transparency window in $\text{Im}\chi^{+,-}(\mathbf{q}, \omega)$ which is approximately $\omega \simeq 2\Delta_0$. In this region a sharp delta-like peak appears in the imaginary part of the susceptibility if the resonance condition $1 + J_{\mathbf{q}}\text{Re}\chi_0^{+,-}(\mathbf{q}, \omega) + \text{Re}\Pi(\mathbf{q}, \omega) + \text{Re}Z(\mathbf{q}, \omega) = 0$ (see Eq. (13)) is fulfilled. Our calculations indicate that for $\text{YBa}_2\text{Cu}_3\text{O}_7$ ($\text{Bi}_2\text{Sr}_2\text{CaCu}_2\text{O}_8$) the value of the gap parameter should be $\Delta_0 = 24$ meV (25 meV). The corresponding values of the superexchange parameter are determined as $J_1 = 90$ meV (110 meV). For these values the resonance condition is fulfilled and a clear peak appears in the imaginary part of the susceptibility near $\omega \simeq 41$ meV, for both materials. In Fig. 2 we display the calculated momentum and frequency dependence of the imaginary part of the susceptibility. Note that the height of the resonance peak depends on the artificially introduced quasiparticle damping Γ , therefore the values of

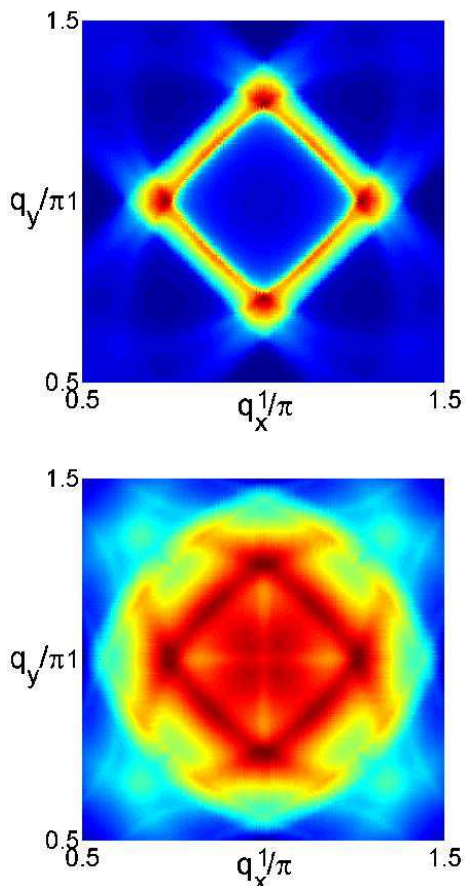


Figure 3: Intensity plot of the imaginary part of the susceptibility $Im\chi^{+,-}(\mathbf{q}, \omega)$ near \mathbf{Q} for $YBa_2Cu_3O_7$ (top) and $Bi_2Sr_2CaCu_2O_8$ (bottom) for $\omega = 30$ meV.

$Im\chi^{+,-}(\mathbf{q}, \omega)$ in Fig. 2 are arbitrary. Furthermore, the experimentally reported²⁷ downward dispersion branch for $YBa_2Cu_3O_7$ with respect to ω is reproduced by our model calculations as can be seen from an inspection of Fig. 2 (top). We would like to point out that for the $Bi_2Sr_2CaCu_2O_8$ compound we do not find a similar dispersion branch. There are, however, no experiments available which would allow a comparison.

Let us now turn to the examination of magnetic excitations at lower frequency, where measurements²⁸ in the $YBaCuO$ compounds indicate well defined incommensurability in the magnetic excitation spectrum. For the material $Bi_2Sr_2CaCu_2O_8$, however, the data sets²⁹ are inconclusive due to experimental difficulty. Here we report significant differences in the low frequency excitations for the materials $YBa_2Cu_3O_7$ and $Bi_2Sr_2CaCu_2O_8$. Similar conclusions were reached previously by Norman³⁰ in the conventional weak-coupling scenario. In Fig. 3 we show an intensity plot of the imaginary part of the susceptibility around the antiferromagnetic wave vector \mathbf{Q} calculated for $\omega = 30$ meV, for both materials. By examination of the figure we conclude that for $YBa_2Cu_3O_7$ the

model calculations match the experimental observation²⁸ of incommensurability. For the $Bi_2Sr_2CaCu_2O_8$ compound, however, our results indicate that the incommensurability of the magnetic excitations is much weaker than in $YBa_2Cu_3O_7$ due to the difference in the Fermi surface topology. This result could be tested by further experiments.

IV. NMR ANALYSIS

A. Knight shift

In order to calculate the Knight shift in the superconducting state we need to calculate the susceptibility in the limit $\mathbf{q} \rightarrow 0$, $\omega = 0$. The BCS susceptibility $\chi_0^{+,-}(\mathbf{q}, \omega)$ converts to the Yosida result³¹

$$\chi_0^{+,-}(\mathbf{q} \rightarrow 0, \omega = 0) \simeq \frac{P\beta}{N} \sum_{\mathbf{k}} \frac{\partial f(E_{\mathbf{k}})}{\partial E_{\mathbf{k}}} = \chi_P. \quad (18)$$

The functions $\Pi(\mathbf{q}, \omega)$ and $Z(\mathbf{q}, \omega)$ are approximated as

$$\begin{aligned} \Pi(\mathbf{q} \rightarrow 0, \omega = 0) &\simeq \frac{1}{N} \sum_{\mathbf{k}} f(E_{\mathbf{k}}) \\ &\quad - \frac{P\beta}{N} \sum_{\mathbf{k}} t_{\mathbf{k}} \frac{\partial f(E_{\mathbf{k}})}{\partial E_{\mathbf{k}}} \\ &\simeq \frac{\delta}{P} - \frac{P\beta}{N} \sum_{\mathbf{k}} t_{\mathbf{k}} \frac{\partial f(E_{\mathbf{k}})}{\partial E_{\mathbf{k}}} \end{aligned} \quad (19)$$

and

$$Z(\mathbf{q} \rightarrow 0, \omega = 0) \simeq P. \quad (20)$$

In the long-wave limit therefore the susceptibility is given by the simple expression

$$\chi^{+,-}(\mathbf{q} \rightarrow 0, \omega = 0) = \frac{\chi_P}{1 + P + \delta/P + (2J_1 - \mu/P)\chi_P}. \quad (21)$$

With the help of this relation the spin shift can be calculated according to

$$K_s \propto A\chi^{+,-}(\mathbf{q} \rightarrow 0, \omega = 0), \quad (22)$$

where A represents the appropriate hyperfine coupling constant. Note that this expression refers to the spin contribution to the magnetic shift. In addition there is an orbital (chemical) shift which, however, is independent of the temperature. We will calculate the temperature dependence of the normalized spin shifts $K_s(T)/K_s(T_c)$. In this way the hyperfine coupling constants in Eq. (22)

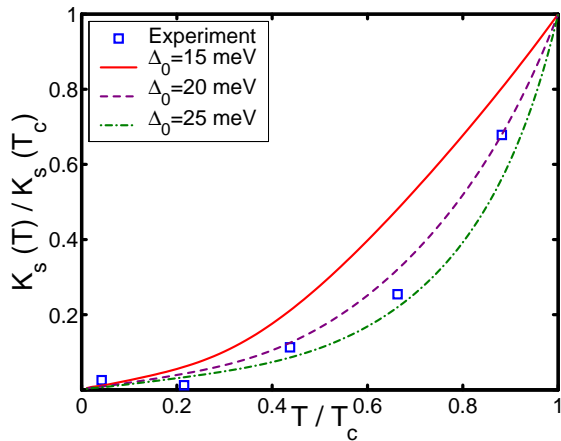


Figure 4: Temperature dependence of the reduced spin shift in $\text{YBa}_2\text{Cu}_3\text{O}_7$ for no exchange interaction ($J_1 = 0$ eV). The experimental points are taken from Barrett et al.³².

cancel out, simplifying our analysis. Furthermore, note that the quasiparticle damping is $\Gamma \rightarrow 0^+$. In Fig. 4 we display the calculated temperature dependence of the spin shifts for $\text{YBa}_2\text{Cu}_3\text{O}_7$, along with the experimental points of Barrett et al.³², for vanishing superexchange interaction $J_1 = 0$ eV and different values of the gap parameter Δ_0 . We observe that below T_c the spin shifts depend strongly on the magnitude of the gap parameter Δ_0 . This behavior has also been found for the RPA susceptibility^{5,6}.

Next we consider how the spin shift depends on the superexchange interaction J_1 . In Fig. 5 the calculated spin shifts for different values of the superexchange interaction parameter J_1 are shown. We see that the temperature dependence of the Knight shift does not significantly change by adjusting the parameter J_1 . Also, contrary to the RPA scenario, the superexchange coupling J_1 reduces the rapid decrease of the Knight shift. By analysis of the figure we conclude that the optimal set of parameters to describe the experimentally observed temperature dependence of the spin shift for $\text{YBa}_2\text{Cu}_3\text{O}_7$ is $\Delta_0 = 24$ meV and $J_1 = 90$ meV for the given Fermi surface. These values are in perfect agreement with those determined from the fit to neutron scattering experiments in the previous section.

Let us now turn to the examination of the spin shift in the $\text{Bi}_2\text{Sr}_2\text{CaCu}_2\text{O}_8$ compound. Experimental results indicate a similar behaviour as in the $\text{YBa}_2\text{Cu}_3\text{O}_7$ material: the spin shift decreases rapidly upon entering the superconducting state. The calculated spin shifts also show a similar dependence on the model parameters Δ_0 and J_1 . We will not repeat the analysis of these dependences and show instead in Fig. 6 the final result of our calculations for the spin shift in $\text{Bi}_2\text{Sr}_2\text{CaCu}_2\text{O}_8$ along with the experimental points of Ishida et al.³³. The parameters used for the calculation are $\Delta_0 = 24$ meV and $J_1 = 110$ meV. We notice that again these values almost coincide with those

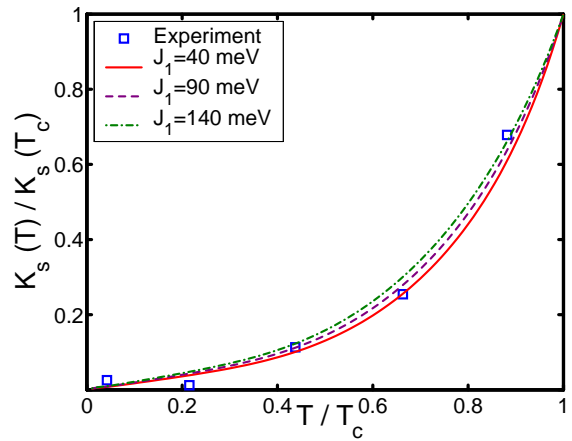


Figure 5: Temperature dependence of the reduced spin shift in $\text{YBa}_2\text{Cu}_3\text{O}_7$. The energy gap is $\Delta_0 = 24$ meV. The experimental points are taken from Barrett et al.³².

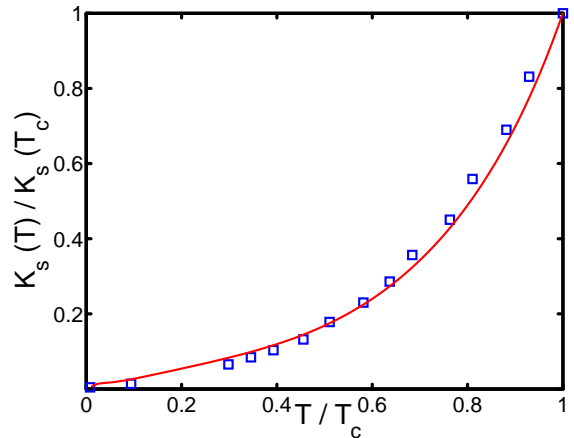


Figure 6: Temperature dependence of the reduced spin shift in $\text{Bi}_2\text{Sr}_2\text{CaCu}_2\text{O}_8$. The experimental points are taken from Ishida et al.³³.

determined by the analysis of neutron scattering experiments in this compound. By examination of the figure we see that the calculated temperature dependence of spin shift gives a satisfactory fit to the experimental data.

Finally we conclude that it is possible to account for both the neutron scattering resonance peak and the temperature dependence of the spin shift in the superconducting state of $\text{YBa}_2\text{Cu}_3\text{O}_7$ and $\text{Bi}_2\text{Sr}_2\text{CaCu}_2\text{O}_8$ consistently within the same set of parameters for each material. Next, we calculate the temperature dependence of dynamical NMR quantities, the spin-spin and spin-lattice relaxation rates.

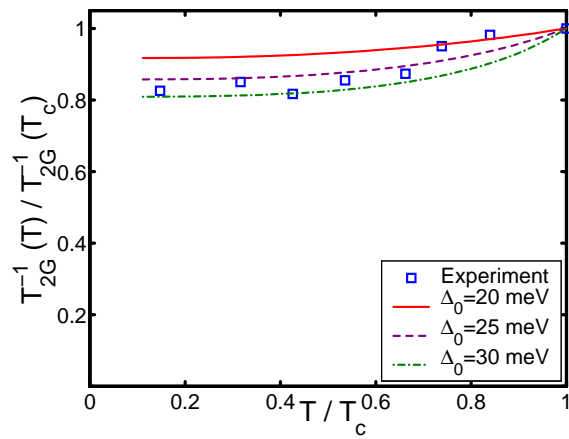


Figure 7: Temperature dependence of the spin–spin relaxation rate in $\text{YBa}_2\text{Cu}_3\text{O}_7$ for no exchange interaction ($J_1 = 0$ eV). The experimental points are taken from Stern et al.³⁵.

B. Spin–spin relaxation

The nuclear spin–spin relaxation rate is calculated from the expression³⁴

$$T_{2G}^{-2} \propto \left[\frac{1}{N} \sum_{\mathbf{q}} {}^{63}F_{\parallel}(\mathbf{q})^2 (Re\chi^{+,-}(\mathbf{q}, \omega = 0))^2 - \left(\frac{1}{N} \sum_{\mathbf{q}} {}^{63}F_{\parallel}(\mathbf{q}) Re\chi^{+,-}(\mathbf{q}, \omega = 0) \right)^2 \right], \quad (23)$$

where ${}^{63}F_{\parallel}(\mathbf{q}) = [A_{\parallel} + 2B(\cos(q_x) + \cos(q_y))]^2$ is the hyperfine form factor. The values of the hyperfine coupling constants are taken as $B \simeq 0.4 \mu\text{eV}$ and $A_{\parallel} \simeq -4B$. The spin–spin relaxation rate allows us to study the real part of the susceptibility $Re\chi^{+,-}(\mathbf{q}, \omega = 0)$ near the antiferromagnetic wave vector \mathbf{Q} . We will calculate the temperature dependence of the normalized spin–spin relaxation rate $T_{2G}^{-1}(T)/T_{2G}^{-1}(T_c)$ in the same way as we analyzed the Knight shifts. Note that for the evaluation of the spin–spin relaxation, the real part of the susceptibility is calculated by taking the quasiparticle damping $\Gamma \rightarrow 0^+$. Otherwise, due to the behavior of the coherence factors, a large increase in the spin–spin relaxation rate occurs near T_c upon entering the superconducting state as has been discussed in Ref.³⁴.

In Fig. 7 we display the calculated spin–spin relaxation rates for $\text{YBa}_2\text{Cu}_3\text{O}_7$ along with experimental points from Stern et al.³⁵ for no superexchange interaction $J_1 = 0$ eV. We observe that the results show a similar temperature dependence as in the RPA approach⁶. Generally, the temperature dependence of the spin–spin relaxation rate is less sensitive to the change of the gap parameter than the spin shift. We see that for the hypothetical case of no interaction we can account for the observed temperature dependence of the spin–spin relax-

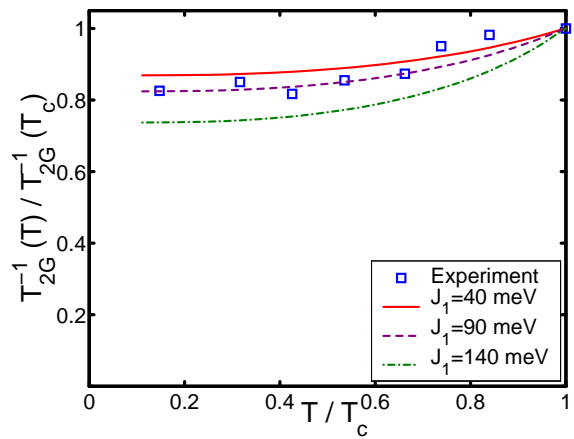


Figure 8: Temperature dependence of the spin–spin relaxation rate in $\text{YBa}_2\text{Cu}_3\text{O}_7$. The energy gap is $\Delta_0 = 22$ meV. The experimental points are taken from Stern et al.³⁵.

ation rate. Next we wish to study the behavior of the spin–spin relaxation for different values of the superexchange interaction parameter J_1 .

In Fig. 8 the temperature dependence of the spin–spin relaxation rate is shown for various values of the superexchange interaction parameter J_1 . We see that we get a reasonable agreement with the data using the parameter values $\Delta_0 = 22$ meV and $J_1 = 90$ meV. The magnitudes of these parameters are in agreement with those obtained by the analysis of neutron scattering and NMR spin shift experiments for $\text{YBa}_2\text{Cu}_3\text{O}_7$.

Concerning the $\text{Bi}_2\text{Sr}_2\text{CaCu}_2\text{O}_8$ compound our calculations indicate a very similar behaviour as in $\text{YBa}_2\text{Cu}_3\text{O}_7$, if we utilize the parameter values from the previous sections $\Delta_0 = 24$ meV and $J_1 = 110$ meV. Unfortunately the spin–spin relaxation rate has not yet been measured in $\text{Bi}_2\text{Sr}_2\text{CaCu}_2\text{O}_8$, thus we have no basis for comparison with experiments.

C. Spin–lattice relaxation

The nuclear spin–lattice relaxation rate is calculated according to the expression³⁶

$$\alpha T_{1\beta}^{-1} \propto \frac{T}{N} \sum_{\mathbf{q}, \beta'} \alpha F_{\beta'}(\mathbf{q}) \lim_{\omega \rightarrow 0} \frac{Im\chi^{+,-}(\mathbf{q}, \omega)}{\omega}, \quad (24)$$

where β denotes the field direction and β' are the directions orthogonal to the field. Furthermore α designates the nucleus under consideration.

In order to calculate the imaginary part of the spin susceptibility $Im\chi^{+,-}(\mathbf{q}, \omega \rightarrow 0)$ we introduced a finite quasiparticle broadening $\Gamma = 3k_B T_c \simeq 2$ meV, following the analysis of Bulut and Scalapino⁵. Furthermore, the form factors in Eq. (24) are given by

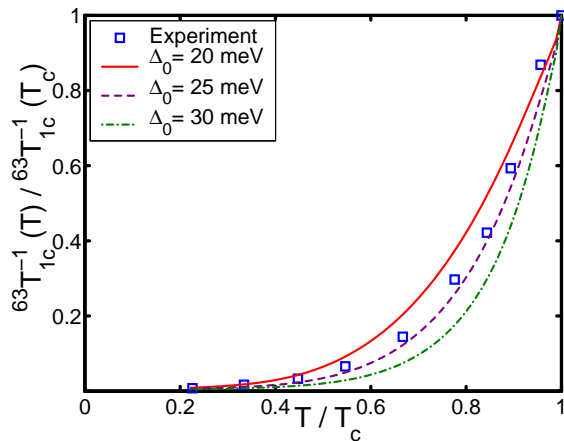


Figure 9: Temperature dependence of the spin–lattice relaxation rate in $\text{YBa}_2\text{Cu}_3\text{O}_7$ for no exchange interaction ($J_1 = 0$ eV). The experimental points are taken from Takigawa et al.³⁷.

$$\begin{aligned} {}^{63}F_{\beta}(\mathbf{q}) &= [A_{\beta} + 2B(\cos(q_x) + \cos(q_y))]^2, \\ {}^{17}F_{\beta}(\mathbf{q}) &= 2(C_{\beta_1}^2 \cos^2(q_x/2) + C_{\beta_2}^2 \cos^2(q_y/2)). \end{aligned} \quad (25)$$

The values of the hyperfine coupling constants are taken as $B \simeq 0.4 \mu\text{eV}$, $A_{\parallel} \simeq -4B$, $A_{\perp} \simeq 0.75B$, $C_{\parallel} \simeq 0.6B$, and $C_{\perp} \simeq 0.32B$.

In Fig. 9 we display the calculated spin–lattice relaxation rates for $\text{YBa}_2\text{Cu}_3\text{O}_7$ along with the experimental points of Takigawa et al.³⁷, when the superexchange interaction is $J_1 = 0$ eV. We observe that the temperature dependence varies strongly when adjusting the gap parameter Δ_0 . As for the spin shift and spin–spin relaxation rate calculations it is possible to fit the experimental data even without taking into account the interaction.

Next we consider the effect of the superexchange parameter J_1 . In Fig. 10 the spin–lattice relaxation rate is shown for different values of J_1 . We note that upon changing the values of J_1 the spin–lattice relaxation rate T_{1c}^{-1} changes the same way as it does in the RPA case if the parameter value of the effective Coulomb interaction U_e is changed. Namely, the parameter J_1 has no significant impact on the temperature dependence of the spin–lattice relaxation rate in the superconducting state. Upon further examination of the figure we see that we get a reasonable agreement with experimental observation using the parameter values $\Delta_0 = 22$ meV and $J_1 = 90$ meV. These parameters agree with those we determined before in the previous Sections.

Next we examine the spin–lattice relaxation rate in the $\text{Bi}_2\text{Sr}_2\text{CaCu}_2\text{O}_8$ compound. Upon changing the model parameters Δ_0 and J_1 the spin–lattice relaxation behaves much the same way as in $\text{YBa}_2\text{Cu}_3\text{O}_7$. We show in Fig. 11 the final result of our calculations of the spin–lattice

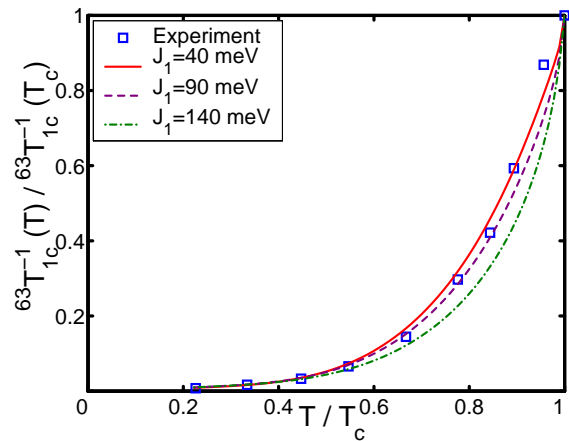


Figure 10: Temperature dependence of the spin–lattice relaxation rate in $\text{YBa}_2\text{Cu}_3\text{O}_7$. The energy gap is $\Delta_0 = 22$ meV. The experimental points are taken from Takigawa et al.³⁷.

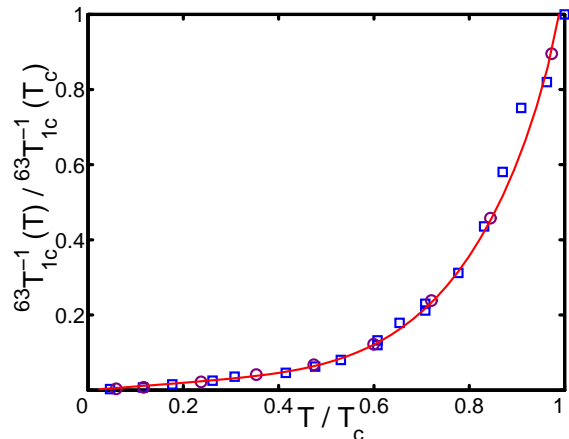


Figure 11: Temperature dependence of the spin–lattice relaxation rate in $\text{Bi}_2\text{Sr}_2\text{CaCu}_2\text{O}_8$. The experimental points are taken from Ishida et al.³³ (squares) and Takigawa et al.³⁸ (circles).

relaxation rate in $\text{Bi}_2\text{Sr}_2\text{CaCu}_2\text{O}_8$, along with the experimental points of Ishida et al.³³ (squares) and Takigawa et al.³⁸ (circles). The parameters used for the calculation are $\Delta_0 = 23$ meV and $J_1 = 110$ meV. Note that the values of these parameters are again almost the same as those that we used before when we analyzed neutron scattering and spin shift experiments. A particularly interesting feature can be found when comparing the spin–lattice relaxation rates in $\text{YBa}_2\text{Cu}_3\text{O}_7$ and $\text{Bi}_2\text{Sr}_2\text{CaCu}_2\text{O}_8$ at low temperatures. A close inspection of the corresponding figures (Fig. 10 and Fig. 11) shows that in the former case ${}^{63}T_{1c}^{-1}(T)$ practically vanishes at temperatures $T < 20$ K, while in the latter case the relaxation rate seems to vanish only at $T \simeq 0$ K. Note that both of these dependences are reproduced by the model calculations.

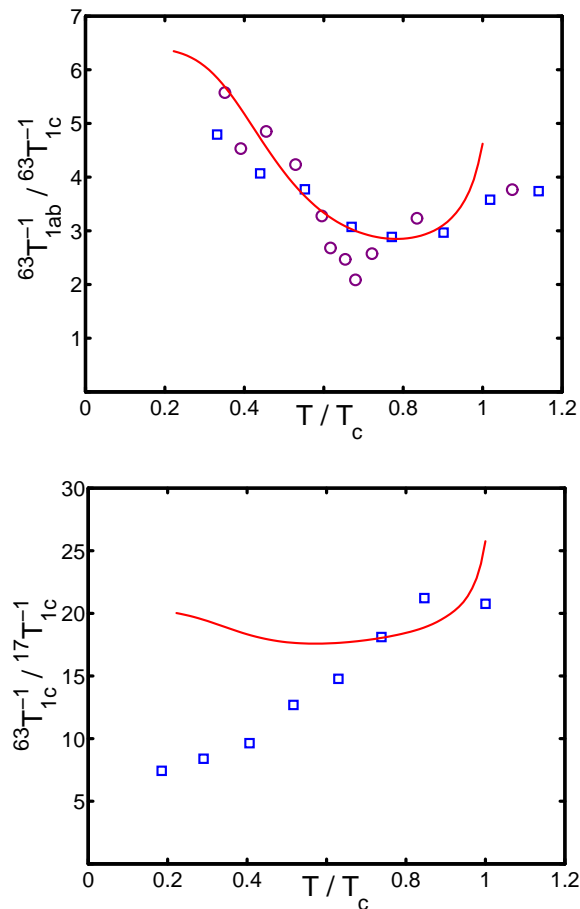


Figure 12: Temperature dependence of the anisotropy ratios ${}^{63}T_{1c}^{-1}/{}^{17}T_{1c}^{-1}$ and ${}^{63}T_{1ab}^{-1}/{}^{63}T_{1c}^{-1}$ in $\text{YBa}_2\text{Cu}_3\text{O}_7$ (squares). Data for $\text{YBa}_2\text{Cu}_4\text{O}_8$ are also shown for comparison (circles).

We are also interested in the anisotropy ratios ${}^{63}T_{1ab}^{-1}/{}^{63}T_{1c}^{-1}$ and ${}^{63}T_{1c}^{-1}/{}^{17}T_{1c}^{-1}$ measured in $\text{YBa}_2\text{Cu}_3\text{O}_7$. Experimental evidence^{39,40,41} points toward a field dependence of these quantities. Our theoretical results have to be compared with data in zero or small external fields. We display the calculated anisotropy ratios in Fig. 12. The experimental points for ${}^{63}T_{1c}^{-1}/{}^{17}T_{1c}^{-1}$ are from Martindale et al.³⁹, whereas those for ${}^{63}T_{1ab}^{-1}/{}^{63}T_{1c}^{-1}$ are taken from Takigawa et al.⁴⁰ (squares). For comparison we also plotted the anisotropy in the $\text{YBa}_2\text{Cu}_4\text{O}_8$ compound (circles) measured by Bankay et al.⁴¹. For the calculation we used the same parameters as before, $\Delta_0 = 22$ meV and $J_1 = 90$ meV. We see that we can account for the anisotropy ratio ${}^{63}T_{1ab}^{-1}/{}^{63}T_{1c}^{-1}$, but it is not possible to reproduce the temperature dependence of the ratio ${}^{63}T_{1c}^{-1}/{}^{17}T_{1c}^{-1}$. Our results for the weak-field anisotropy ratio ${}^{63}T_{1ab}^{-1}/{}^{63}T_{1c}^{-1}$ for $\text{YBa}_2\text{Cu}_3\text{O}_7$ agree with the weak-coupling calculations of Bulut and Scalapino⁵, which are based on a square Fermi surface with nearest neighbour hopping only. However, our calculations disagree with the analysis of Mack et al.⁶, where the

Fermi surface for $\text{YBa}_2\text{Cu}_3\text{O}_7$ was assumed to be quite different (similar to that which we used here to describe the $\text{Bi}_2\text{Sr}_2\text{CaCu}_2\text{O}_8$ compound). Therefore we conclude that the Fermi surface topology plays an important role in the description of the weak-field anisotropy ratio ${}^{63}T_{1ab}^{-1}/{}^{63}T_{1c}^{-1}$. Note that the experimentally reported weak-field ratio ${}^{63}T_{1c}^{-1}/{}^{17}T_{1c}^{-1}$ could also not be reproduced within previous weak-coupling RPA calculations^{5,6}.

V. CONCLUSIONS

In summary we have determined the spin susceptibility in cuprates within a special Hubbard model which includes strong correlation effects. It has been found that the susceptibility in the strong-coupling limit is different from the standard Pauli-Lindhard formula. In particular, two correction functions were determined in the superconducting state. The first one, $\Pi(\mathbf{q}, \omega)$, found originally by Hubbard and Jain¹³ in the normal state, originates from the anticommutator rule which is modified due to the Coulomb repulsion, whereas the function $Z(\mathbf{q}, \omega)$ has its origin in the fast fluctuations of the localized spins and was previously discussed by Zavidonov and Brinkmann¹¹ for the normal state.

We analyzed inelastic neutron scattering and NMR data in the superconducting state of the optimally doped high- T_c superconductors $\text{YBa}_2\text{Cu}_3\text{O}_7$ and $\text{Bi}_2\text{Sr}_2\text{CaCu}_2\text{O}_8$. In our analysis we have taken into account the experimentally measured topology of the Fermi surface, which is quite different for these two materials. We found that on the whole the results within the strong-coupling and weak-coupling limits agree with each other. Based on the results of our numerical calculations we conclude that strong correlation effects, i.e. the effect of the functions $\Pi(\mathbf{q}, \omega)$, $Z(\mathbf{q}, \omega)$ on the susceptibility can be modeled in the weak-coupling approach by an appropriate redefinition²⁵ of the effective Coulomb interaction parameter U_e . In particular, the non-physical value of U_e in the weak-coupling limit (sometimes $U_e \geq t$) becomes understandable. In terms of our model this can be explained by the impact of the $\Pi(\mathbf{q}, \omega)$ function, which is of the order of $t\chi_0^{+,-}(\mathbf{q}, \omega)$. As concerns the $Z(\mathbf{q}, \omega)$ function, our calculations show that if it is not included, the numerical values of $\text{Im}\chi^{+,-}(\mathbf{q}, \omega)$ can for some set of parameters become negative, implying the importance of this correction.

In the framework of the singlet-correlated band model we found it possible to describe the available experimental data in the optimally doped $\text{YBa}_2\text{Cu}_3\text{O}_7$ and $\text{Bi}_2\text{Sr}_2\text{CaCu}_2\text{O}_8$ compounds within one set of model parameters for each material. These optimal sets of parameters are given by $\Delta_0 = 23$ meV ($\pm 5\%$), $J_1 = 90$ meV for $\text{YBa}_2\text{Cu}_3\text{O}_7$ and $\Delta_0 = 24$ meV ($\pm 5\%$), $J_1 = 110$ meV for $\text{Bi}_2\text{Sr}_2\text{CaCu}_2\text{O}_8$. The only experiment which could not be reproduced is the temperature dependence of the

weak-field anisotropy ratio $^{63}T_{1c}^{-1}/^{17}T_{1c}^{-1}$ in $\text{YBa}_2\text{Cu}_3\text{O}_7$. As concerns the $\text{Bi}_2\text{Sr}_2\text{CaCu}_2\text{O}_8$ material, more experimental data would be desirable to test our model further, for example low energy inelastic neutron scattering and spin-spin relaxation rate measurements.

Acknowledgments

This work is supported by the Swiss National Science Foundation. M. Eremin was partially supported by the

Russian RFFI (grant No. 03 02 17430) and Superconductivity program. We would like to thank M. Mali and J. Roos for fruitful discussions.

-
- ¹ N. Bulut, D. W. Hone, D. J. Scalapino and N. E. Bickers, *Phys. Rev. B* **41**, 1797 (1990)
- ² N. Bulut, D. Hone, D. J. Scalapino and N. E. Bickers, *Phys. Rev. Lett.* **64**, 2723 (1990)
- ³ N. Bulut and D. J. Scalapino, *Phys. Rev. Lett.* **67**, 2898 (1991)
- ⁴ N. Bulut and D. J. Scalapino, *Phys. Rev. Lett.* **68**, 706 (1992)
- ⁵ N. Bulut and D. J. Scalapino, *Phys. Rev. B* **45**, 2371 (1992)
- ⁶ F. Mack, M. L. Kubic, M. Mehring, *Physica C* **295**, 136 (1998)
- ⁷ D. K. Morr and D. Pines, *Phys. Rev. Lett.* **81**, 1086 (1998)
- ⁸ F. Onufrieva and P. Pfeuty, *Phys. Rev. B* **65**, 054515 (2002)
- ⁹ Z. Y. Weng, D. N. Sheng and C. S. Ting, *Phys. Rev. B* **52**, 637 (1995)
- ¹⁰ I. Sega, P. Prelovsek and J. Bonca, *Phys. Rev. B* **68**, 054524 (2003)
- ¹¹ A. Yu. Zavidonov and D. Brinkmann, *Phys. Rev. B* **58**, 12486 (1998)
- ¹² M. Eremin, I. Eremin and S. Varlamov, *Phys. Rev. B* **64**, 214512 (2001)
- ¹³ J. Hubbard and K. P. Jain, *J. Phys. C ser. 2*, vol 1, 1650 (1968)
- ¹⁴ I. Eremin, O. Kamaev and M. V. Eremin, *Phys. Rev. B* **69**, 094517 (2004)
- ¹⁵ F. C. Zhang and T. M. Rice, *Phys. Rev. B* **37**, R3759 (1988)
- ¹⁶ M. Eremin, S. G. Solov'yanov and S. V. Varlamov, *JETP* **85**, 963 (1997)
- ¹⁷ M. R. Norman, *Phys. Rev. B* **63**, 092509 (2000)
- ¹⁸ M. Eschrig and M. R. Norman, *Phys. Rev. B* **67**, 144503 (2003)
- ¹⁹ P. Bourges, L. P. Regnault, Y. Sidis, C. Vettier, *Phys. Rev. B* **53**, 876 (1996)
- ²⁰ H. A. Mook, M. Yethiraj, G. Aeppli, T. E. Mason, T. Armstrong, *Phys. Rev. Lett.* **70**, 3490 (1993)
- ²¹ H. Fong, P. Bourges, Y. Sidis, L. P. Regnault, A. Ivanov, G. D. Gu, N. Koshizuka, B. Keimer, *Nature* **398**, 588 (1999)
- ²² H. He, Y. Sidis, P. Bourges, G. D. Gu, A. Ivanov, N. Koshizuka, B. Liang, C. T. Lin, L. P. Regnault, E. Schoen-herr, B. Keimer, *Phys. Rev. Lett.* **86**, 1610 (2001)
- ²³ V. Hinkov, S. Pailhes, P. Bourges, Y. Sidis, A. Ivanhov, A. Kulakov, C. T. Lin, D. P. Chen, C. Bernhard and B. Keimer, *Nature* **430**, 650-654 (2004)
- ²⁴ S. Pailhes et al. , *Phys. Rev. Lett.* **91**, 237002 (2003)
- ²⁵ I. Eremin, D. Manske, *Phys. Rev. Lett.* **94**, 067006 (2005)
- ²⁶ J. Brinckmann and P. A. Lee, *Phys. Rev. B* **65**, 014502 (2002)
- ²⁷ D. Reznik, P. Bourges, L. Pintschovius, Y. Endoh, Y. Sidis, T. Masui and S. Tajima, *Phys. Rev. Lett.* **93**, 207003 (2004)
- ²⁸ H. A. Mook, Pengcheng Dai, S. M. Hayden, G. Aeppli, T. G. Perring, F. Dogan, *Nature* **395**, 580 (1998)
- ²⁹ H. A. Mook, F. Dogan, B. C. Chakoumakos, *cond-mat/9811100*
- ³⁰ M. R. Norman, *Phys. Rev. B* **61**, 14751 (2000)
- ³¹ K. Yosida, *Phys. Rev.* **110**, 769 (1958)
- ³² S. E. Barrett, D. J. Durand, C. H. Pennington, C. P. Slichter, T. A. Friedmann, J. P. Rice and D. M. Ginsberg, *Phys. Rev. B* **41**, 6283 (1990)
- ³³ K. Ishida, K. Yoshida, T. Mito, Y. Tokunaga, Y. Kitaoka, K. Asayama, A. Nakayama, J. Shimoyama, K. Kishio, *Phys. Rev. B* **58**, R5960 (1998)
- ³⁴ D. Thelen and D. Pines, *Phys. Rev. B* **49**, 3528 (1994)
- ³⁵ R. Stern, M. Mali, J. Roos and D. Brinkmann, *Phys. Rev. B* **51**, 15478 (1995)
- ³⁶ T. Moriya, *J. Phys. Soc. Jpn* **18** 516-523 (1963)
- ³⁷ M. Takigawa, A. P. Reyes, P. C. Hammel, J. D. Thompson, R. H. Heffner, Z. Fisk, and K. C. Ott, *Phys. Rev. B* **43**, 247 (1991)
- ³⁸ M. Takigawa and D. B. Mitzi, *Phys. Rev. Lett.* **73**, 1287 (1994)
- ³⁹ J. A. Martindale, S. E. Barrett, K. E. O'Hara, C. P. Slichter, W. C. Lee and D. M. Ginsberg, *Phys. Rev. B* **47**, R9155 (1993)
- ⁴⁰ M. Takigawa, J. L. Smith and W. L. Hults, *Phys. Rev. B* **44**, R7764 (1991)
- ⁴¹ M. Bankay, M. Mali, J. Roos, I. Mangelschots and D. Brinkmann, *Phys. Rev. B* **46**, R11228 (1992)